Pattern Recognition Letters 33 (2012) 677–684

Contents lists available at SciVerse ScienceDirect

Pattern Recognition Letters

journal homepage: www.elsevier.com/locate/patrec

A calibration method for paracatadioptric camera from sphere images

Huixian Duan *, Yihong Wu

National Laboratory of Pattern Recognition, Institute of Automation, Chinese Academy of Sciences, 100190 Beijing, China

ARTICLE INFO

Article history:
Received 9 March 2011
Available online 29 December 2011
Communicated by B. Kamgar-Parsi

Keywords:
Paracatadioptric camera calibration
Sphere images
Antipodal sphere images

ABSTRACT

For paracatadioptric camera, the estimation of intrinsic parameters from sphere images is still an open and challenging problem. In this paper, we propose a calibration method for paracatadioptric camera based on sphere images, which only requires that the projected contour of parabolic mirror is visible on the image plane in one view. We have found that, under central catadioptric camera, a sphere is projected to two conics on the image plane, which are defined as a pair of antipodal sphere images. The conic that is visible on the image plane is called the sphere image, while the other invisible conic is called the antipodal sphere image. In the other aspect, according to the image formation of central catadioptric camera, these two conics can also be considered as the projections of two parallel circles on the viewing sphere by a virtue camera. That is to say, if three pairs of antipodal sphere images are known, central catadioptric camera can be directly calibrated by the calibration method based on two parallel circles. Therefore, the problem of calibrating central catadioptric camera is transferred to the estimations of sphere images and their antipodal sphere images. Based on this idea, we first initialize the intrinsic parameters of the camera by the projected contour of parabolic mirror, and use them to initialize the antipodal sphere images. Next, we study properties of several pairs of antipodal sphere images under paracatadioptric camera. Then, these properties are used to optimize sphere images and their antipodal sphere images, so as to calibrate the paracatadioptric camera. Experimental results on both simulated and real image data have demonstrated the effectiveness of our method.

1. Introduction

In many applications in computer vision, such as robot navigation and virtual reality, a camera with a quite large field of view is required. Since the conventional camera has a very limited field of view. One effective way to enhance its field of view is to combine the camera with mirrors, which is referred to as catadioptric image formation. Catadioptric system can be classified into two groups, central and noncentral, based on the uniqueness of an effective viewpoint (Baker and Nayer, 1999). For central catadioptric system, the calibration of camera is still a prerequisite for its applications. In the literature, its calibration methods can be classified into the following five categories:

1. Self-calibration. These methods just use point correspondences in multiple views, without needing to know either the 3D location of space points or camera locations. Kang (2000) used the consistency of pairwise tracked point features across a sequence of images to develop a reliable calibration method for paracatadioptric camera.
2. Based on 3D points. These methods need to know 3D world coordinates. Aliaga (2001) relaxed the assumption of ideal paracatadioptric system and introduced a camera model to estimate the intrinsic and extrinsic parameters for paracatadioptric camera. Vasseur and Mouaddib (2004) determined intrinsic parameters of any central catadioptric camera by a nonlinear method with 3D space points. Wu and Hu (2005) established three kinds of interesting invariant equations from 1D, 2D and 3D scene points under central catadioptric camera model and used them to calculate the principal point with a quasi-linear method. Bastanlar et al. (2008) proposed a method based on the direct linear transformation using lifted coordinates to calibrate any central catadioptric camera.
3. Based on 2D points. These methods use a 2D calibration pattern with control points. Scaramuzza et al. (2006) assumed that the image projection function could be described by a Taylor series expansion whose coefficients were estimated by solving a two-step least squares linear minimization problem. Based on this assumption, they proposed a technique to calibrate single viewpoint omnidirectional cameras. Mei and Rives (2007) also presented a flexible calibration method for omnidirectional single viewpoint sensors from planar grids. But this method was based on an exact theoretical projection function and some parameters as distortion were added to consider real-world errors.

* Corresponding author. Tel.: +86 10 62542946.
E-mail address: hxduan@nlpr.ia.ac.cn (H. Duan).

0167-8655/$ - see front matter © 2011 Elsevier B.V. All rights reserved.
doi:10.1016/j.patrec.2011.12.012

Deng et al. (2007) used the explicit relationship between the central catadioptric model and the pinhole model, then the intrinsic and extrinsic parameters were estimated by nonlinear optimization. Zhang et al. (2009) studied the geometry of central catadioptric of a set of lines and presented a practical calibration method for central catadioptric cameras by manually labeling the corners on planar grids.

4. Based on lines. These methods only use the images of lines, without any knowledge of metric information. Geyer and Daniilidis (1999, 2002) calibrated paracatadioptric camera using a single view of two sets of parallel lines or a single view of three lines. Barreto and Araujo (2002) studied the projective invariant properties of line images and showed that any central catadioptric camera could be fully calibrated from an image of three or more lines. Ying and Zha (2005) used Hough transform to detect line images, which ensured that all detected conics must belong to a line image family related to certain intrinsic parameters. Vandeportaele et al. (2006) replaced the algebraic distance with a geometric one to slightly improve the performance of the calibration method proposed in (Geyer and Daniilidis, 2002) and they allowed to deal with lines that were projected to straight lines and circular arcs in an unified manner. Wu et al. (2006) presented a calibration method for para-catadioptric-like cameras from lines without conic fitting. They derived linear constraints on the intrinsic parameters through a shift from the central catadioptric model to the pinhole model. Recently, Wu et al. (2008) established a set of linear constraints on the catadioptric parameters from line images using the projection of points. Based on these linear constraints, any central catadioptric camera could be calibrated without prior knowledge.
5. Based on sphere. These methods only use the images of spheres in the scene, without any knowledge of metric information. Ying and Hu (2004) proposed a calibration method based on spheres. They proved that the projection of a sphere could provide two invariants, from which, constraint equations for the intrinsic parameters of central catadioptric camera were derived. Since this calibration method is nonlinear. Ying and Zha (2008) proposed a linear method to calibrate camera from sphere images, by introducing the modified image of the absolute conic. In case of paracatadioptric camera, these calibration methods are degenerate, thus cannot be used to compute the camera intrinsic parameters.

In order to make calibration based on spheres for central catadioptric cameras complete, in this paper, we propose a calibration method for paracatadioptric camera based on spheres, which only requires the projected contour of parabolic mirror is visible on the image plane in one view. Under central catadioptric, we know that the projection of a sphere on the viewing sphere is two circles, which are projected to two conics on the image plane by a virtual camera. That is, the projection of a sphere is two conics. These two conics are defined as a pair of antipodal sphere images, and can be considered as the projections of two parallel circles on the viewing sphere by a virtual camera. One of them is visible on the image plane and called the sphere image, while the other one is invisible which we called the antipodal sphere image. Therefore, if three pairs of antipodal sphere image are known, the paracatadioptric camera can be calibrated from the method proposed in (Wu et al., 2004, 2006).

Based on the idea above, firstly, we initialize the intrinsic parameters of the camera by the projected contour of parabolic mirror, and use them to initialize the antipodal sphere images. Next, we study the properties of several pairs of antipodal sphere images and obtain some constraints, which must be satisfied by the equations of sphere images and their antipodal sphere images. Then, the obtained constraints are used to optimize the sphere images and their antipodal sphere images. Finally, these optimized sphere images and their antipodal sphere images are used to calibrate the paracatadioptric camera. Compared with the initialized intrinsic parameters, the calibration accuracy has been improved greatly by our method. Extensive experiments have shown the effectiveness of our method.

This paper is organized as follows: Section 2 reviews the unified sphere model introduced by Geyer and Daniilidis (2001) and some related works. Section 3 studies the properties of K ($K \geqslant 3$) pairs of antipodal sphere images. In Section 4, the calibration algorithm for paracatadioptric camera from sphere images is described in detail. Experimental results are shown in Section 5. Finally, Section 6 presents some concluding remarks.

2. Preliminaries

A bold letter denotes a vector or a matrix. Without special explanation, a vector is homogenous coordinates. In the following, we briefly review the image formation for central catadioptric camera introduced in (Geyer and Daniilidis, 2001), the antipodal image points and their properties proposed in (Wu et al., 2008) as well as the calibration method for pinhole camera from two parallel circles (Wu et al., 2004).

2.1. Central catadioptric projection model

Geyer and Daniilidis (2001) showed that the central catadioptric imaging process is equivalent to the following two-step mapping by a sphere (see Fig. 1): Firstly, under the viewing sphere coordinate system $O - X_sY_sZ_s$, a 3D point $\boldsymbol{X} = (x,y,z)^T$ is projected to a point $\boldsymbol{X_s} = (x_s,y_s,z_s)^T$ on the unit sphere centered at the viewpoint $\boldsymbol{O}$; Secondly, the point $\boldsymbol{X_s}$ is projected to a point $\boldsymbol{m}$ on the image plane $\boldsymbol{\Pi}$ by a pinhole camera through the perspective center $\boldsymbol{O_c}$. The image plane is perpendicular to the line going through the viewpoints $\boldsymbol{O}$ and $\boldsymbol{O_c}$. Let the intrinsic parameter matrix of the pinhole camera be

$$\boldsymbol{K}_c = \begin{pmatrix} r_c f_c & s & u_0 \\ 0 & f_c & v_0 \\ 0 & 0 & 1 \end{pmatrix},$$

where r_c is the aspect ratio, f_c is the effective focal length, $(u_0, v_0, 1)^T$ denoted as $\boldsymbol{p}$ is the principal point, and s is the skew factor. Then, the imaging process of a space point $\boldsymbol{X}$ to $\boldsymbol{m}$ can be described as:

$$\alpha \boldsymbol{m} = \boldsymbol{K}_c \left(\frac{\mathbf{R}\mathbf{X} + \boldsymbol{t}}{\|\mathbf{R}\mathbf{X} + \boldsymbol{t}\|} + \xi \boldsymbol{e} \right), \tag{1}$$

where α is a scalar, $\boldsymbol{R}$ is a 3×3 rotation matrix, $\boldsymbol{t}$ is a 3-vector of translation, $\|\cdot\|$ denotes the norm of vector in it, $\boldsymbol{e} = (0,0,1)^T$, and ξ is the mirror parameter, i.e. the distance from $\boldsymbol{O}$ to $\boldsymbol{O_c}$. The mirror is a paraboloid if $\xi = 1$, an ellipsoid or hyperboloid if $0 < \xi < 1$, and a plane if $\xi = 0$.

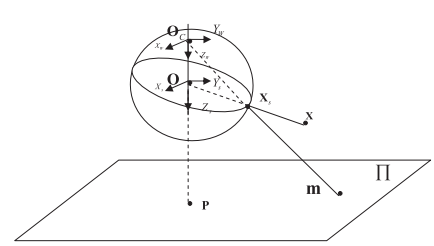

Fig. 1. The image formation of a point.

2.2. The antipodal image points

Under central catadioptric camera, Wu et al. (2008) gave the definition of antipodal image points and derived their properties as follows:

Definition 1. $\{m, m'\}$ is called a pair of antipodal image points if they could be images of two end points of a diameter of the viewing sphere (see Fig. 2).

Proposition 1. *If $\{m, m'\}$ is a pair of antipodal image points under a central catadioptric camera, we have:*

$$\frac{1+\sqrt{1+\tau \boldsymbol{m}^T\boldsymbol{\varpi}\boldsymbol{m}}}{\boldsymbol{m}^T\boldsymbol{\varpi}\boldsymbol{m}}\boldsymbol{m}+\frac{1+\sqrt{1+\tau \boldsymbol{m}'^T\boldsymbol{\varpi}\boldsymbol{m}'}}{\boldsymbol{m}'^T\boldsymbol{\varpi}\boldsymbol{m}'}\boldsymbol{m}'=2\boldsymbol{p}, \tag{2}$$

where $\tau=(1-\xi^2)/\xi^2$, $\boldsymbol{\varpi}=\boldsymbol{K}_c^{-T}\boldsymbol{K}_c^{-1}$. In the case of parabolic mirror, (2) is simplified as

$$\frac{1}{\boldsymbol{m}^T\boldsymbol{\varpi}\boldsymbol{m}}\boldsymbol{m}^T\boldsymbol{\varpi}\boldsymbol{m}+\frac{1}{\boldsymbol{m}'^T\boldsymbol{\varpi}\boldsymbol{m}'}\boldsymbol{m}'^T\boldsymbol{\varpi}\boldsymbol{m}'=\boldsymbol{p}. \tag{3}$$

2.3. The calibration method for pinhole camera from two parallel circles

Wu et al. (2004) presented a calibration method for the pinhole camera from three views of two parallel images. Here, we briefly review the calibration steps.

Step 1: In each view, determine the images of two parallel circles: $\boldsymbol{C}_{+i}$ and $\boldsymbol{C}_{-i}$, $i = 1, 2, 3$.
Step 2: Solve the common solutions of $\boldsymbol{C}_{+i}$, $\boldsymbol{C}_{-i}$ in each view, $i = 1, 2, 3$.
Step 3: Find out the images of the circular points from the solved common solutions of $\boldsymbol{C}_{+i}$, $\boldsymbol{C}_{-i}$, $i = 1, 2, 3$.
Step 4: Set up the equations on the intrinsic parameters $\boldsymbol{\omega}=\boldsymbol{K}_C^{-T}\boldsymbol{K}_C^{-1}$ from the images of circular points found out in Step 3.
Step 5: Solve out $\boldsymbol{\omega}$ from the equations in Step 4 bysingular value decomposition method, and then do Cholesky decomposition and inverse the result to obtain the intrinsic parameters $\boldsymbol{K}_C$.

3. Properties of K ($K \geqslant 3$) pairs of antipodal sphere images under paracatadioptric camera

Ying and Hu (2004) gave that the projection of a sphere under paracatadioptric camera is two conics (see Fig. 3), which are defined as a pair of antipodal sphere images. The conic, being visible on the image plane, is called the sphere image. And the other conic, being invisible on the image plane, is called the antipodal sphere image. In addition, from the image formation, we notice that the projection of a sphere is two parallel circles on the viewing sphere, because the unite normal vectors of the base planes containing them are parallel. Thus, the projection of a sphere can be considered as the projections of two parallel circles on the viewing sphere by a virtue camera.

Under paracatadioptric camera, the representations of two conics, being the projection of a sphere, are (Ying and Hu, 2004):

$$\boldsymbol{C}_{\pm}=\boldsymbol{K}_c^{-T}\boldsymbol{C}'_{\pm}\boldsymbol{K}_c^{-1}, \tag{4}$$

where

$$\boldsymbol{C}'_{\pm}=\begin{pmatrix}(\pm d_0-n_z)^2 & 0 & (\pm d_0-n_z)n_x\\ 0 & (\pm d_0-n_z)^2 & (\pm d_0-n_z)n_y\\ (\pm d_0-n_z)n_x & (\pm d_0-n_z)n_y & (d_0^2-n_z^2)\end{pmatrix}.$$

$(n_x, n_y, n_z)^T$ is the unite normal vector of the base plane containing circle on the viewing sphere, and d_0 is the distance from the origin $\boldsymbol{O}$ to the base plane. $\boldsymbol{C}_+$ represents the sphere image and $\boldsymbol{C}_-$ represents the antipodal sphere image.

For K ($K \geqslant 3$) views, a sphere in space is projected to K pairs of conic curves $\boldsymbol{C}_{\pm i}$

$$\boldsymbol{C}_{\pm i}=\begin{pmatrix}a_{\pm i} & b_{\pm i} & d_{\pm i}\\ b_{\pm i} & c_{\pm i} & e_{\pm i}\\ d_{\pm i} & e_{\pm i} & f_{\pm i}\end{pmatrix}, \quad i=1,2,3,\ldots,K. \tag{5}$$

Expanding the right side of (4), we obtain

$$\begin{cases} b_{\pm i}=\frac{k_2}{k_1}a_{\pm i},\\ c_{\pm i}=\left(\frac{k_2^2}{k_1^2}+\frac{k_3^2}{k_1^2}\right)a_{\pm i},\\ d_{\pm i}=\left(\frac{k_4}{k_1}+\frac{1}{k_1}\frac{n_{xi}}{\pm d_{0i}-n_{zi}}\right)a_{\pm i},\\ e_{\pm i}=\left(\frac{k_2}{k_1}\left(\frac{k_4}{k_1}+\frac{1}{k_1}\frac{n_{xi}}{\pm d_{0i}+n_{zi}}\right)+\frac{k_3}{k_1}\left(\frac{k_5}{k_1}+\frac{1}{k_1}\frac{n_{yi}}{\pm d_{0i}+n_{zi}}\right)\right)a_{\pm i},\\ f_{\pm i}=\left(\frac{k_4}{k_1}\left(\frac{k_4}{k_1}+2\frac{1}{k_1}\frac{n_{xi}}{\pm d_{0i}+n_{zi}}\right)+\frac{k_5}{k_1}\left(\frac{k_5}{k_1}+2\frac{1}{k_1}\frac{n_{yi}}{\pm d_{0i}+n_{zi}}\right)\right.\\ \qquad\left.+\frac{1}{k_1^2}\frac{\pm d_{0i}+n_{zi}}{\pm d_{0i}-n_{zi}}\right)a_{\pm i}, \end{cases} \tag{6}$$

where

$$\begin{cases} k_1=\frac{1}{r_c f_c},\\ k_2=-\frac{s}{r_c f_c^2},\\ k_3=\frac{1}{f_c},\\ k_4=\frac{s v_0}{r_c f_c^2}-\frac{u_0}{r_c f_c},\\ k_5=-\frac{v_0}{f_c}. \end{cases} \tag{7}$$

From the first two expressions in (6), we know that

$$\begin{cases} \frac{b_{\pm 1}}{a_{\pm 1}}=\frac{b_{\pm 2}}{a_{\pm 2}}=\frac{b_{\pm 3}}{a_{\pm 3}}=\cdots=\frac{b_{\pm K}}{a_{\pm K}}=\frac{k_2}{k_1},\\ \frac{c_{\pm 1}}{a_{\pm 1}}=\frac{c_{\pm 2}}{a_{\pm 2}}=\frac{c_{\pm 3}}{a_{\pm 3}}=\cdots=\frac{c_{\pm K}}{a_{\pm K}}=\frac{k_2^2}{k_1^2}+\frac{k_3^2}{k_1^2}. \end{cases} \tag{8}$$

From the first expression in (8) it follows that $\alpha_{+i}=\alpha_{-i}=0$ for $i=2,3,\ldots,K$, with $\alpha_{\pm i}$ obtained from the first expression in (9). Moreover, using the second expression in (8) in a similar manner, we obtain $\beta_{+i}=\beta_{-i}=0$ for $i=2,3,\ldots,K$ with $\beta_{\pm i}$ given by the second expression in (9).

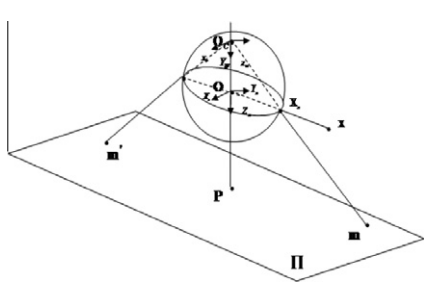

Fig. 2. $\{\boldsymbol{m}, \boldsymbol{m}'\}$ is a pair of antipodal image points.

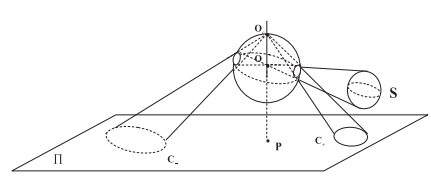

Fig. 3. The image formation of a sphere.

$$\begin{cases} \alpha_{\pm i} = a_{\pm 1} b_{\pm i} - a_{\pm i} b_{\pm 1}, & i = 2, 3, \ldots, K. \\ \beta_{\pm i} = a_{\pm 1} c_{\pm i} - a_{\pm i} c_{\pm 1}, & i = 2, 3, \ldots, K. \end{cases} \tag{9}$$

In addition, from the expressions in (6) and (7), after some manipulations, we have

$$\begin{cases} \frac{k_2}{k_1} = \frac{b_{\pm i}}{a_{\pm i}}, \\ \frac{k_3}{k_1} = \sqrt{\frac{c_{\pm i}}{a_{\pm i}} - \frac{b_{\pm i}^2}{a_{\pm i}^2}}, \\ \frac{k_4}{k_1} = -\frac{b_{\pm i}}{a_{\pm i}} v_0 - u_0, \\ \frac{k_5}{k_1} = -\sqrt{\frac{c_{\pm i}}{a_{\pm i}} - \frac{b_{\pm i}^2}{a_{\pm i}^2}} v_0. \end{cases} \tag{10}$$

In each view, denote

$$\frac{1}{k_1} \frac{n_{xi}}{\pm d_{0i} - n_{zi}} = \Delta_1, \quad \frac{1}{k_1} \frac{n_{yi}}{\pm d_{0i} - n_{zi}} = \Delta_2, \quad \frac{1}{k_1^2} \frac{\pm d_{0i} + n_{zi}}{\pm d_{0i} - n_{zi}} = \Delta_3.$$

From the third expression in (6) and (10), we have

$$\Delta_1 = \frac{d_{\pm i}}{a_{\pm i}} - \frac{k_4}{k_1} = \frac{d_{\pm i}}{a_{\pm i}} + \frac{b_{\pm i}}{a_{\pm i}} v_0 - u_0. \tag{11}$$

What's more, substituting (10) and (11) into the fourth expression in (6), solving Δ_2 as

$$\Delta_2 = \left(\frac{e_{\pm i}}{a_{\pm i}} - \frac{b_{\pm i}}{a_{\pm i}} \frac{d_{\pm i}}{a_{\pm i}} \right) \Big/ \sqrt{\frac{c_{\pm i}}{a_{\pm i}} - \frac{b_{\pm i}^2}{a_{\pm i}^2}} + \sqrt{\frac{c_{\pm i}}{a_{\pm i}} - \frac{b_{\pm i}^2}{a_{\pm i}^2}} v_0. \tag{12}$$

Next, substituting (10)–(12) into the fifth term in (6),after some manipulations (see Appendix A) then

$$\Delta_3 = u_0^2 + 2 \frac{b_{\pm i}}{a_{\pm i}} u_0 v_0 + \frac{c_{\pm i}}{a_{\pm i}} v_0^2 + 2 \frac{d_{\pm i}}{a_{\pm i}} u_0 + 2 \frac{e_{\pm i}}{a_{\pm i}} v_0 + \frac{f_{\pm i}}{a_{\pm i}}. \tag{13}$$

For a pair of antipodal sphere images, from (11) we have

$$\begin{cases} \frac{1}{k_1} \frac{n_{xi}}{d_{0i} - n_{zi}} = \frac{d_{+i}}{a_{+i}} + \frac{b_{+i}}{a_{+i}} v_0 - u_0, \\ \frac{1}{k_1} \frac{n_{xi}}{-d_{0i} - n_{zi}} = \frac{d_{-i}}{a_{-i}} + \frac{b_{-i}}{a_{-i}} v_0 - u_0. \end{cases} \tag{14}$$

In (14), the first expression is divided by the second expression, then

$$\frac{d_{0i} - n_{zi}}{-d_{0i} - n_{zi}} = \frac{\frac{d_{+i}}{a_{+i}} + \frac{b_{+i}}{a_{+i}} v_0 - u_0}{\frac{d_{-i}}{a_{-i}} + \frac{b_{-i}}{a_{-i}} v_0 - u_0}, \tag{15}$$

denote $\boldsymbol{v}_{\pm i}^1 = (-a_{\pm i}, b_{\pm i}, d_{\pm i})$, then (15) changes into

$$\frac{d_{0i} - n_{zi}}{-d_{0i} - n_{zi}} = \frac{\frac{1}{a_{+i}} \boldsymbol{v}_{+i}^1 \boldsymbol{p}}{\frac{1}{a_{-i}} \boldsymbol{v}_{-i}^1 \boldsymbol{p}}, \tag{16}$$

where $\boldsymbol{p}$ is the principal point.

Similarly, from (12) and (13), we have

$$\begin{cases} \frac{d_{0i} - n_{zi}}{-d_{0i} - n_{zi}} = \frac{\frac{1}{a_{+i}^2} \boldsymbol{v}_{+i}^2 \boldsymbol{p}}{\frac{1}{a_{-i}^2} \boldsymbol{v}_{-i}^2 \boldsymbol{p}}. \\ \frac{(d_{0i} - n_{zi})^2}{(d_{0i} + n_{zi})^2} = \frac{\frac{1}{a_{-i}} \boldsymbol{p}^T \boldsymbol{C}_{-i} \boldsymbol{p}}{\frac{1}{a_{+i}} \boldsymbol{p}^T \boldsymbol{C}_{+i} \boldsymbol{p}}. \end{cases} \tag{17}$$

where $\boldsymbol{v}_{\pm i}^2 = (0,\ a_{\pm i} c_{\pm i} - b_{\pm i}^2,\ a_{\pm i} e_{\pm i} - b_{\pm i} d_{\pm i})$.

Therefore, in each view, from (16) and (17), we obtain that

$$\begin{cases} \eta_i = \frac{\frac{1}{a_{+i}} \boldsymbol{v}_{+i}^1 \boldsymbol{p}}{\frac{1}{a_{-i}} \boldsymbol{v}_{-i}^1 \boldsymbol{p}} - \frac{\frac{1}{a_{+i}^2} \boldsymbol{v}_{+i}^2 \boldsymbol{p}}{\frac{1}{a_{-i}^2} \boldsymbol{v}_{-i}^2 \boldsymbol{p}} = 0. \\ \chi_i = \left(\frac{\frac{1}{a_{+i}} \boldsymbol{v}_{+i}^1 \boldsymbol{p}}{\frac{1}{a_{-i}} \boldsymbol{v}_{-i}^1 \boldsymbol{p}} \right)^2 - \frac{\frac{1}{a_{-i}} \boldsymbol{p}^T \boldsymbol{C}_{-i} \boldsymbol{p}}{\frac{1}{a_{+i}} \boldsymbol{p}^T \boldsymbol{C}_{+i} \boldsymbol{p}} = 0. \end{cases} \tag{18}$$

(18) is equivalent to

$$\begin{cases} \eta_i = a_{+i} \boldsymbol{v}_{+i}^1 \boldsymbol{p} \boldsymbol{v}_{-i}^2 \boldsymbol{p} - a_{-i} \boldsymbol{v}_{-i}^1 \boldsymbol{p} \boldsymbol{v}_{+i}^1 \boldsymbol{p} = 0, & i = 1, 2, 3, \ldots, K. \\ \chi_i = a_{-i}^3 (\boldsymbol{v}_{+i}^1 \boldsymbol{p})^2 \boldsymbol{p}^T \boldsymbol{C}_{+i} \boldsymbol{p} - a_{+i}^3 (\boldsymbol{v}_{-i}^1 \boldsymbol{p})^2 \boldsymbol{p}^T \boldsymbol{C}_{-i} \boldsymbol{p} = 0, & i = 1, 2, 3, \ldots, K. \end{cases} \tag{19}$$

Finally, from (13), we have

$$\begin{cases} \frac{1}{k_1^2} \frac{d_{0i} + n_{zi}}{d_{0i} - n_{zi}} = \frac{1}{a_{+i}} \boldsymbol{p}^T \boldsymbol{C}_{+i} \boldsymbol{p}, \\ \frac{1}{k_1^2} \frac{-d_{0i} + n_{zi}}{-d_{0i} - n_{zi}} = \frac{1}{a_{-i}} \boldsymbol{p}^T \boldsymbol{C}_{-i} \boldsymbol{p}, \end{cases} \tag{20}$$

the first expression is multiplied by the second expression in (20), then

$$\frac{1}{k_1^4} = \frac{1}{a_{+i} a_{-i}} \boldsymbol{p}^T \boldsymbol{C}_{+i} \boldsymbol{p} \boldsymbol{p}^T \boldsymbol{C}_{-i} \boldsymbol{p}. \tag{21}$$

Thus, in different views, from (21), we obtain

$$v_i = a_{+i} a_{-i} \boldsymbol{p}^T \boldsymbol{C}_{+1} \boldsymbol{p} \boldsymbol{p}^T \boldsymbol{C}_{-1} \boldsymbol{p} - a_{+1} a_{-1} \boldsymbol{p}^T \boldsymbol{C}_{+i} \boldsymbol{p} \boldsymbol{p}^T \boldsymbol{C}_{-i} \boldsymbol{p} = 0, \quad i = 2, 3, \ldots, K. \tag{22}$$

If a set of K conic curves corresponds to the paracatadioptric projection of a sphere in K views, then (9), (19) and (22) are true. Therefore, they can be used to optimize the equations of antipodal sphere images.

4. Calibration algorithm for paracatadioptric cameras

It is well known that a pinhole camera can be calibrated from two parallel circles (Wu et al., 2004). As we have described before, under central catadioptric camera, the projection of a sphere can be considered as the projections of two parallel circles on the viewing sphere by a virtual camera. Therefore, if K ($K \geqslant 3$) pairs of antipodal sphere images are known, central catadioptric camera can be calibrated. In this section, using the properties of antipodal sphere images derived in Section 3, we estimate the equations of sphere images and their antipodal sphere images under paracatadioptric camera, then to calibrate the paracatadioptric camera.

Consider the projections of a sphere under paracatadioptric camera in K views. For each sphere image $\boldsymbol{C}_{+i}$ in (5), it corresponds to a set of image points $\boldsymbol{m}_j^i$, with $i = 1,2,3,\ldots,K$ and $j = 1,2,3,\ldots,N_i$ ($N_i \geqslant 5$). Now, we estimate the equations $\boldsymbol{C}_{+i}$ of sphere images. Firstly, $\boldsymbol{C}_{+i}$ is initialized by the least squares method. Then, it is optimized by minimizing the following function:

$$\varepsilon = \sum_{i=1}^{K} \sum_{j=1}^{N_i} \boldsymbol{m}_j^{iT} \boldsymbol{C}_{+i} \boldsymbol{m}_j^i + \lambda \left(\sum_{i=2}^{K} \alpha_{+i} + \sum_{i=2}^{K} \beta_{+i} \right). \tag{23}$$

where λ is a Lagrange multiplier. In the following, we determine the equations $\boldsymbol{C}_{-i}$ of antipodal sphere images.

4.1. Estimation of K (K ⩾ 3) antipodal sphere images under paracatadioptric camera

Firstly, we give an initialization of the equations $\boldsymbol{C}_{-i}$, $i = 1,2,3,\ldots,K$. Suppose the projected contour $\boldsymbol{C}$ (a 3×3 matrix) of the parabolic mirror is visible on the image plane in one view and its equation is:

$$\boldsymbol{C} = \begin{pmatrix} a & b & d \\ b & c & e \\ d & e & f \end{pmatrix}.$$

Then, the initial values of r_c, s, u_0, v_0, f_c can be obtained (Ying and Hu, 2004):

$$\begin{cases} r_c = \sqrt{-\frac{b^2}{a^2} + \frac{c}{a}}, \\ s = -\frac{b}{a}, \\ u_0 = \frac{be-cd}{ac-b^2}, \\ v_0 = \frac{bd-ae}{ac-b^2}, \\ f_c = u_0^2 a + 2u_0 v_0 b + v_0^2 c + 2u_0 d + 2v_0 e + f. \end{cases} \tag{24}$$

By the property of antipodal image points shown in (3), we can compute the antipodal image points $\boldsymbol{m}_j^{i'}$ of $\boldsymbol{m}_j^i$ using the obtained intrinsic parameters in (24), $i = 1,2,3,\ldots,K$ and $j = 1,2,3,\ldots,N_i$. Then, estimate $\boldsymbol{C}_{-i}$ using $\boldsymbol{m}_j^{i'}$, $j = 1,2,\ldots,N_i$ by the least squares method.

Next, we optimize the equations $\boldsymbol{C}_{-i}$ of antipodal sphere images through minimizing the following object function:

$$F = \sum_{i=1}^{K} (\eta_i^2 + \chi_i^2) + \sum_{i=2}^{K} (\alpha_{-i}^2 + \beta_{-i}^2 + \nu_i^2). \tag{25}$$

4.2. The calibration method for paracatadioptric camera based on spheres

Our algorithm for calibrating paracatadioptric camera from the projections of a sphere in K views is outlined as follows:

Step 1: Extract the pixels of sphere images in K views and estimate their equations $\boldsymbol{C}_{+i}$ by minimizing the object function (23), $i = 1,2,3,\ldots,K$;
Step 2: In one view, extract the pixels of projected contour of parabolic mirror and determine the equation $\boldsymbol{C}$ by the least squares method;
Step 3: By the method presented in Section 4.1, determine the equations $\boldsymbol{C}_{-i}$ of the antipodal sphere images in K views, $i = 1,2,3,\ldots,K$;
Step 4: Calibrate the intrinsic parameters of paracatadioptric camera by the calibration method shown in Section 2.3.

It is well known that the estimated intrinsic parameters of the camera by the projected contour of parabolic mirror usually are

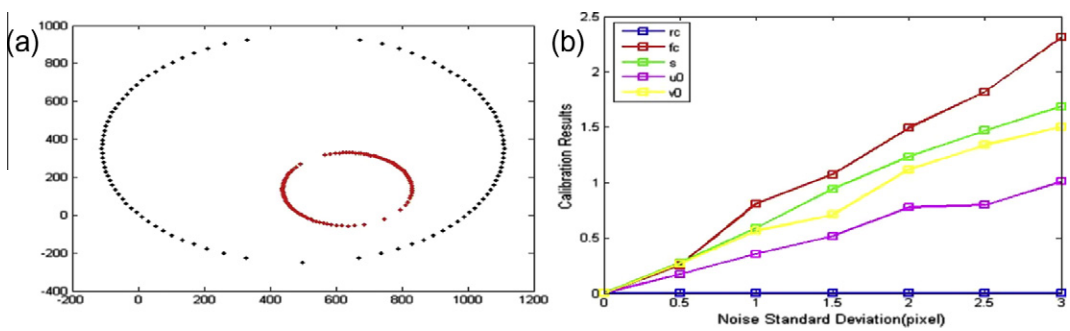

Fig. 4. (a) A simulated sphere image. (b) Calibration results of intrinsic parameters.

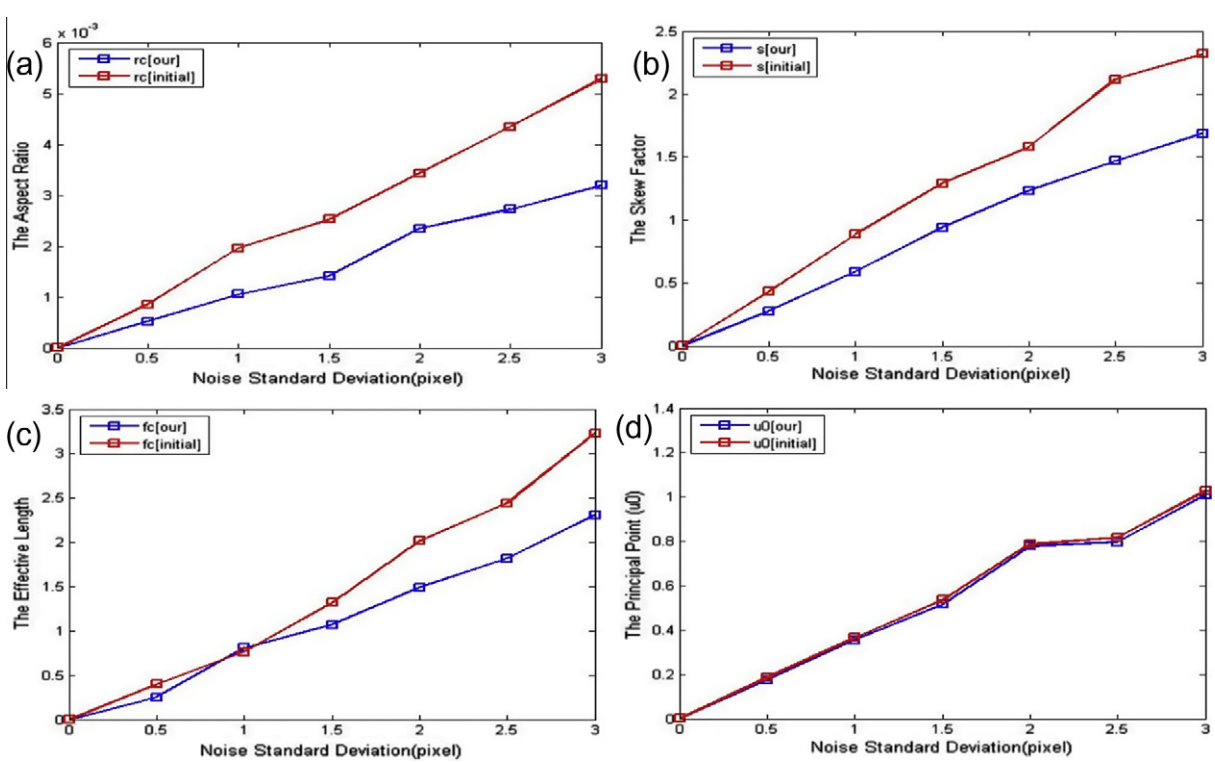

Fig. 5. The comparison between the initial intrinsic paraments and the estimated results by our method. (a)–(d) The comparison of r_c, s, f_c and u_0 respectively.

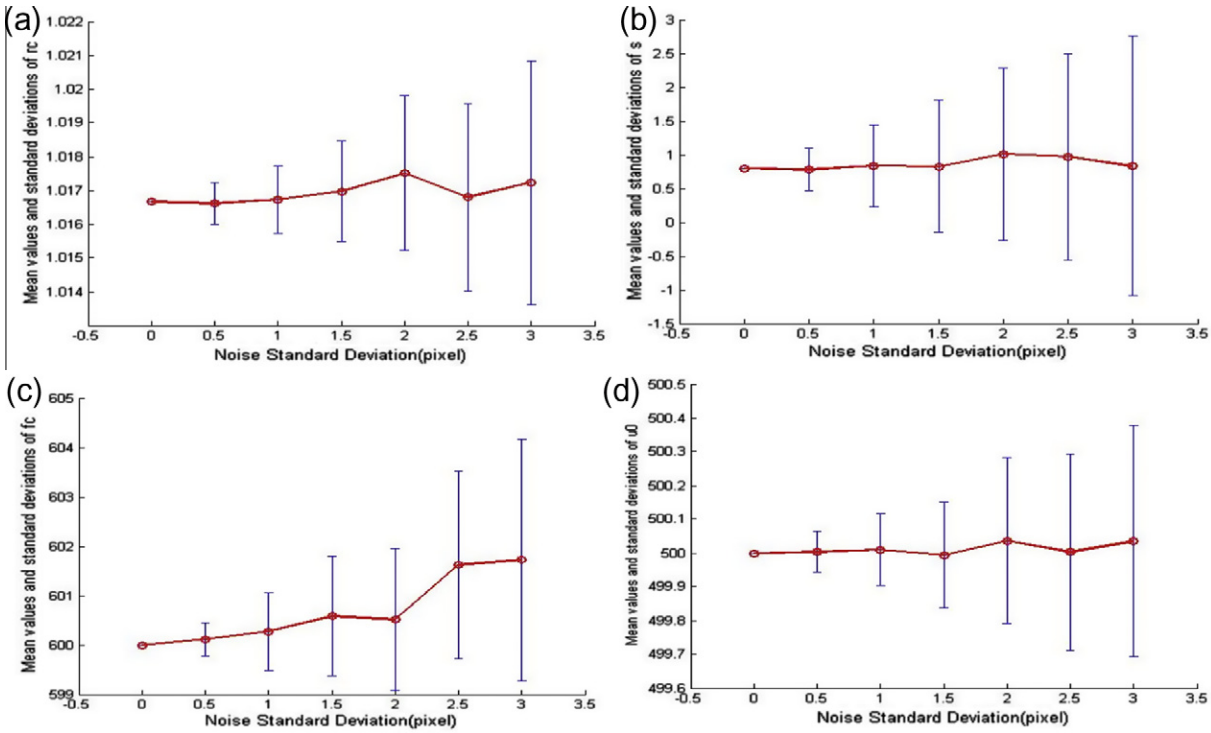

Fig. 6. The simulated results for paracatadioptric camera. (a)–(d) The means and standard deviations of r_c, s, f_c and u_0 respectively.

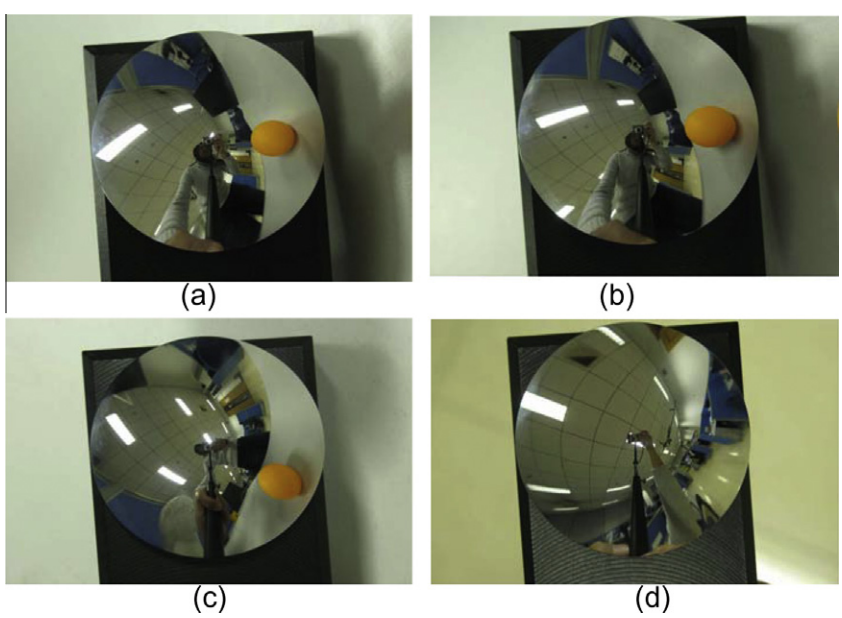

Fig. 7. (a)–(c) Three sphere images used in the real experiments. (d) The test image.

not accurate enough, thus we expect the calibration accuracy can be improved greatly through our method mentioned above. The following experiments show that our method has the performance as expected.

5. Experiments

In this section, we perform a number of experiments with simulated and real images to evaluate the performance of our calibration algorithm.

5.1. Experimental results with simulated data

The simulated camera has the following intrinsic parameter matrix:

$$\boldsymbol{K}_c = \begin{pmatrix} 610 & 0.8 & 500 \\ 0 & 600 & 350 \\ 0 & 0 & 1 \end{pmatrix}, \tag{26}$$

where $(500, 350, 1)^T$ is the principal point $\boldsymbol{p}$, 61/60 is the aspect ratio r_c, 0.8 is the skew factor s and 600 is the effective focal length f_c.

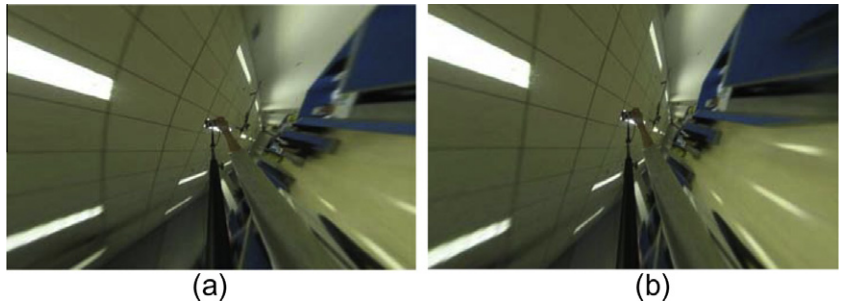

Fig. 8. (a) The rectified image using the initial parameters. (b) The rectified image using the estimated parameters by our method.

The projections of a sphere in three views are generated to calibrate the paracatadioptric camera. One of them is shown in Fig. 4(a), in which the larger conic is the projected contour of parabolic mirror. The projected contour and each sphere image are consisted of 100 points respectively. Gaussian noise with mean 0 and standard deviation σ ranging from 0 to 3 is directly added to each of the points on the sphere images. Because the resolution of the image edge is lower than that of the image center, we add noise with 2σ to the projected contour of parabolic mirror.

We calibrate intrinsic parameters for the paracatadioptric camera using the method proposed in Section 4.2. The estimated parameters are compared with the ground truth and the RMS (Root Mean Square) error is computed over 100 runs of each experiment. Fig. 4(b) shows RMS error of the estimated intrinsic parameters. It can be seen that the calibration results are correct and the variances are almost linear with noise. What's more, Fig. 5 compares the calibration results obtained by our method with the initial intrinsic parameters estimated by the projected contour of parabolic mirror. Since the performances of u_0 and v_0 are very similar, the estimated results for v_0 are not shown here. We seen that our calibration results are more accurate than the initial parameters.

In addition, at each noise level, we perform 100 independent trails. The means and the standard deviations of intrinsic parameters are computed and shown in Fig. 6. Since the performances of u_0 and v_0 are very similar, the estimated results for v_0 are not shown here. From Fig. 6, the results indicate the proposed method is quite correct and stable to the intrinsic parameters.

5.2. Experimental results with real image

Three real images of a ping-pong are used for the real experiment. They are captured by a CANON A640 with a hyperboloid mirror designed by the Center for Machine Perception, Czech technical University. The mirror parameter $\xi = 0.966$ that is close to 1. Here, we approximately regarded it as 1. Three images of a ping-pong are shown in Fig. 7 (a)–(c). The sphere images are extracted using Canny's edge detector. Then, applying the proposed calibration algorithm proposed in Section 4.2, the intrinsic parameters can be estimated. To check the calibration result, we use the estimated intrinsic parameters to rectify the test image shown in Fig. 7 (d). The rectified results are shown in Fig. 8. Fig. 8 (a) gives the rectified result using the initial parameters obtained by (24), and Fig. 8(b) gives the rectified result using the estimated intrinsic parameters by the proposed method. It can be seen that the proposed calibration method is very effective.

6. Conclusion

This paper proposes a calibration method for paracatadioptric camera, which only requires that the projected contour of the parabolic mirror is visible on the image plane in one view. This solves the degeneracy problem in (Ying and Hu, 2004; Ying and Zha, 2008) and makes calibration based on spheres for central catadioptric cameras complete. According to the image formation, we have found that the projection of a sphere can be considered as the projections of two parallel circles on the viewing sphere by a virtual camera. In other words, as long as three projections of these two parallel circles are known, the paracatadioptric camera can be directly calibrated by the method proposed in (Wu et al., 2004). Therefore, firstly, initialize the intrinsic parameters of the camera by the projected contour of parabolic mirror, and use them to initialize the antipodal sphere images. Next, obtain some constraints, which must be satisfied by the equations of sphere images and their antipodal sphere images. Then, such constraints are used to optimize the equations of the projections of two parallel circles so as to achieve the purpose of calibrating the paracatadioptric camera. Both the simulated and real experiments have validated the effectiveness of our method.

Acknowledgements

This work is supported by the National Basic Research Program of China under Grant No. 2012CB316302 and by the National Natural Science Foundation of China under Grant No. 61070107.

Appendix A

We would like to give some derivations for the Eq. (13) in detail. From the fifth expression in (6) follows that

$$\Delta_3 = \frac{f_{\pm i}}{a_{\pm i}} - \left(\frac{k_4}{k_1}\left(\frac{k_4}{k_1} + 2\frac{1}{k_1}\frac{n_{xi}}{\pm d_{0i} + n_{zi}}\right) + \frac{k_5}{k_1}\left(\frac{k_5}{k_1} + 2\frac{1}{k_1}\frac{n_{yi}}{\pm d_{0i} + n_{zi}}\right)\right). \tag{A.1}$$

Substituting (11) and (12) into (A.1) yields

$$\Delta_3 = \frac{f_{\pm i}}{a_{\pm i}} - \left(\frac{k_4}{k_1}\left(2\frac{d_{\pm i}}{a_{\pm i}} - \frac{k_4}{k_1}\right) + \frac{k_5}{k_1}\left(2\left(\frac{e_{\pm i}}{a_{\pm i}} - \frac{k_2}{k_1}\frac{d_{\pm i}}{a_{\pm i}}\right)\Big/\frac{k_3}{k_1} - \frac{k_5}{k_1}\right)\right). \tag{A.2}$$

Substituting the last two expressions in (10) into (A.2) follows that

$$\Delta_3 = \frac{f_{\pm i}}{a_{\pm i}} + 2\frac{d_{\pm i}}{a_{\pm i}}u_0 + u_0^2 + 2\frac{k_2}{k_1}u_0 v_0 + \frac{k_2^2}{k_1^2}v_0^2 + 2\frac{e_{\pm i}}{a_{\pm i}}v_0 + \left(\frac{k_3}{k_1}v_0\right)^2. \tag{A.3}$$

Substituting the first two expressions in (10) into (A.4), then

$$\Delta_3 = u_0^2 + 2\frac{b_{\pm i}}{a_{\pm i}}u_0 v_0 + \frac{c_{\pm i}}{a_{\pm i}}v_0^2 + 2\frac{d_{\pm i}}{a_{\pm i}}u_0 + 2\frac{e_{\pm i}}{a_{\pm i}}v_0 + \frac{f_{\pm i}}{a_{\pm i}}.$$

References

Aliaga, D., 2001. Accurate catadioptric calibration for real-time pose estimation in room-size environments. In: Proc. Internat. Conf. of Computer Vision (ICCV). pp. 127–134.

Baker, S., Nayer, S., 1999. A theory of single-viewpoint catadioptric image formation. Int. J. Comput. Vision 35, 175–196.

Barreto, J., Araujo, H., 2002. Geometry properties of central catadioptric line images. In: Proc. European Conf. of Computer Vision (ECCV). pp. 237–251.
Bastanlar, Y., Puig, L., Sturm, P., Guerrero, J., Barreto, J., 2008. Dlt-like calibration of central catadioptric cameras. In: Proc. Workshop on Omnidirectional Vision, Camera Networks and Non-Classical Cameras.
Deng, X., Wu, F., Wu, Y., 2007. An easy calibration method for central catadioptric cameras. Acta Autom. Sin. 33, 801–808.
Geyer, C., Daniilidis, K., 1999. Catadioptric camera calibration. In: Proc. Internat. Conf. of Computer Vision (ICCV). pp. 398–404.
Geyer, C., Daniilidis, K., 2001. Catadioptric projective geometry. Int. J. Comput. Vision 45, 223–243.
Geyer, C., Daniilidis, K., 2002. Paracatadioptric camera calibration. IEEE Trans. Pattern Anal. Machine Intell. 24, 687–695.
Kang, S., 2000. Catadioptric self-calibration. In: Proc. IEEE Conf. on Computer Vision and Pattern Recognition (CVPR). Vol. 1. pp. 201–207.
Mei, C., Rives, P., 2007. Single view point omnidirectional camera calibration from planar grids. In: Proc. Internat. Conf. on Robotics and Automation (ICRA). pp. 3945–3950.
Scaramuzza, D., Martinelli, A., Siegwart, R., 2006. A flexible technique for accurate omnidirectional camera calibration and structure from motion. In: Proc. Internat. Conf. of Computer Vision (ICCV). pp. 45–52.
Vandeportaele, B., Cattoen, M., Marthon, P., Gurdjos, P., 2006. A new linear calibration method for paracatadioptric cameras. In: Proc. Internat. Conf. on Pattern Recognition (ICPR). Vol. 4. pp. 647–651.
Vasseur, P., Mouaddib, E., 2004. Central catadioptric line detection. In: Proc. British Machine Vision Conference. (BMVC).
Wu, F., Duan, F., Hu, Z., Wu, Y., 2008. A new linear algorithm for calibrating central catadioptric cameras. Pattern Recognit. 41, 3166–3172.
Wu, Y., Hu, Z., 2005. Geometric invariants and applications under catadioptric camera model. In: Proc. Internat. Conf. of Computer Vision (ICCV). pp. 1547–1554.
Wu, Y., Li, Y., Hu, Z., 2006. Easy calibration for para-catadioptric-like camera. In: Proc. Internat. Conf. on Intelligent Robots and Systems. pp. 5719–5724.
Wu, Y., Zhu, H., Hu, Z., Wu, F., 2004. Camera calibration from the quasi-affine invariance of two parallel circles. In: Proc. European Conf. of Computer Vision (ECCV). pp. 190–202.
Wu, Y., Liu, X., Wu, F., Hu, Z., 2006. Coplanar circles, quasi-affine invariance and calibration. Image Vision Comput. 24, 319–326.
Ying, X., Hu, Z., 2004. Catadioptric camera calibration using geometric invariants. IEEE Trans. Pattern Anal. Machine Intell. 26, 1260–1271.
Ying, X., Zha, H., 2005. Simultaneously calibrating catadioptric camera and detecting line features using hough transform. In: Proc. Internat. Conf. on Intelligent Robots and Systems. pp. 412–417.
Ying, X., Zha, H., 2008. Identical projective geometric properties of central catadioptric lines images and sphere images with applications to calibration. Int. J. Comput. Vision 78, 89–105.
Zhang, L., Du, X., Zhu, Y., Liu, J., 2009. Central catadioptric camera calibration with single image. In: Proc. Internat. Conf. on Acoustics, Speech and Signal Processing.